Journal of Electrostatics 109 (2021) 103550

Contents lists available at ScienceDirect

Journal of Electrostatics

journal homepage: www.elsevier.com/locate/elstat

Designing electrode profiles with the equipotential method

Wanchun Wei *

Los Alamos National Laboratory, Los Alamos, NM 87545, USA
Kellogg Radiation Laboratory, California Institute of Technology, Pasadena, CA 91125, USA

ARTICLE INFO

Keywords:
3D electrode design
Equipotential method
Uniform field electrode
Electrodes to hold a dielectric object
Electrode of low symmetry
Electrode of irregular shape

ABSTRACT

A good electrode design not only produces the goal electric fields, but also eliminates harmful high-field spots that can cause electrical breakdown. In this paper, we present the equipotential method to generate electrode profiles. It is a physical method. The desired field is constructed first by a set of virtual electrodes, and then the equipotential contours naturally become the electrode profiles. We will demonstrate the simple procedures to design uniform field electrodes and recessed electrodes to accommodate dielectric structures. It shows versatility and flexibility in designing electrodes of low symmetry or irregular shapes as well as in complex boundary conditions.

1. Introduction

Uniform field electrodes (UFE) are employed to produce electric fields with uniform strength distribution over a large surface area in many applications, such as in the high-energy electrical discharge chamber of CO_2 lasers or Excimer lasers, in the measurement of breakdown electric fields of various gases, etc. Several analytic or empirical electrode profiles have been reported as designs approximating a true UFE [1–6]. The most commonly used are Rogowski profiles [1,2]. Another well-known set of UFE profiles is generated by analytic formulas that were first derived by Chang [7] and later improved by Ernst [8,9]. These profiles are found to be superior to the Rogowski profiles and others regarding smoothness, compactness and field uniformity. A numerical approach to generate electrode profiles has been pursued by Harrison and Pearson [4–6]. In 1985, Girdinio and his colleagues published a new class of UFE profiles originating from the equipotential contours of parallel plates, and compared them with the then-existing UFE profiles [10]. We call it the equipotential method. But this approach did not become popular perhaps due to lack of generality and computing power at the time. The mainstream methodology is to join curves or shapes into an electrode profile, and then perform a series of subtle adjustments to curvatures either manually or via sophisticated algorithms [11,12] to remove high field spots. Now it might be worthwhile to revisit the equipotential method for UFE profile generation and explore its flexibility in solving complex problems, since (i) computing power has advanced dramatically in the last few decades, (ii) physical modeling software with finite element method (FEM), e.g. COMSOL Multiphysics, has been well-developed and become commercially available, and (iii) computer numerical control (CNC) technology has enabled modern machining equipment to precisely manufacture objects of almost arbitrary shape.

In recent years, UFEs also play important roles in particle physics research [13]. Electrodes of Rogowski profiles have been employed to study the breakdown behavior of noble liquid, such as liquid helium [14], argon and xenon [15], which can be used as target and detection medium in dark matter searches [16,17]. In experiments searching for a non-zero but extremely weak neutron electric dipole moment (nEDM) with ultracold neutrons (UCNs), strong and stable electric fields on the order of tens to a hundred kilovolts per centimeter are required to achieve the goal sensitivity. Dielectric structures in the form of either an annular cylinder or a closed cell have to be sandwiched in between the electrodes so as to confine the space distribution of UCNs in the high field region [18–20]. Distortions of electric fields due to the existence of dielectric structures are inevitable, but a near uniform field in the test region is still highly desired to minimize systematic errors. Since bulk dielectric fully extending against the electrodes induces extremely high fields in any small spacing between the dielectric and metal surfaces, edges of the dielectric are especially vulnerable to breakdown damage. It has been demonstrated that placing the edge of the dielectric structure in a corner formed by the equipotential surface of the electrode is an effective way to reduce the local stress and suppress possibility of electrical breakdown [21–23]. Efforts have been spent on designing electrode profiles with a recess to hold and protect the corners of the dielectric structures. This practice evolved into a new approach of designing electrodes of

* Correspondence to: Kellogg Radiation Laboratory, California Institute of Technology, Pasadena, CA 91125, USA.
E-mail address: wanchun.wei@caltech.edu.

https://doi.org/10.1016/j.elstat.2021.103550
Received 19 October 2020; Received in revised form 8 December 2020; Accepted 4 January 2021
Available online 7 January 2021

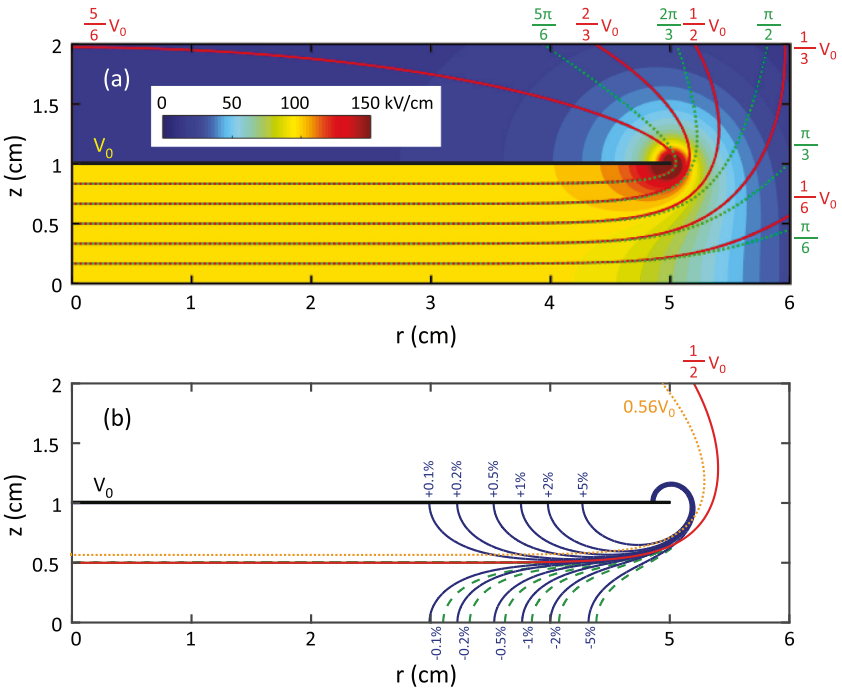

Fig. 1. (a) Equipotential lines and field distribution are plotted in red solid lines and color gradient map, respectively for the parallel plates at $V^{\pm} = \pm 100$ kV with a separation $d = 2$ cm. Only the upper half plane is shown because of symmetry. Various Rogowski profiles are also plotted in green dotted lines as a comparison. (b) Field uniformity of the parallel plates is presented as contours of discrepancies from the uniform field E_0. In general, the discrepancies are positive above the $V_0/2$ equipotential line (in red solid line), and negative below. The field uniformity contours of the $\pi/2$ Rogowski profile are plotted in dashed green line for a comparison. The $0.56V_0$ equipotential line is also plotted in orange dotted line. (For interpretation of the references to color in this figure legend, the reader is referred to the web version of this article.)

complex shape in the presence of dielectric structures and boundary conditions. Below we will present the methodology.

In this paper, we first show how to generate UFE profiles with the equipotential method in Section 2. Section 2.1 reveals that nature of the methodology to obtain Rogowski profiles is the 2D equipotential method; Section 2.2 analyzes the performance of UFE profiles generated by the 3D equipotential method; and Section 2.3 extends the method to create closed UFE profiles by manipulating the equipotential contour. In Section 3, we demonstrate how to generate recessed electrode profiles to accommodate different geometries of dielectric structures with a new technique, named the molding technique. Finally in Section 4, the advantages of the method and implications of its applications will be summarized. All of the electrostatic modeling is done with FEM in COMSOL Multiphysics. This paper only focuses on demonstrating the equipotential method but not optimization of the electrode performance.

2. Equipotential method to generate UFE profiles

Ideally, a perfectly uniform electric field is created by a pair of infinite parallel plates. In reality, finite width of the plates results in deviation of the field strength near the edge. In order to achieve a uniform field in the central region, a large ratio of the plate width w to the separation d is required. Yet, sharp curvatures at the edges of the plates result in fringe fields much stronger than the central region and cause discharge or breakdown in experiments. Therefore, smoothly rounding the edges of the parallel plates became an intuitive option in the UFE design. This is usually done by joining curves and tuning their curvature heuristically or via sophisticated algorithms. We call it the curve-joining method. Alternatively, the equipotential method offers a different approach. In electrostatics, field lines are always orthogonal to equipotential contours, as well as to the surface profile of a conductor. Therefore, converting any equipotential contour into a conductor boundary and setting it to the potential value thereof will not change the field distribution in the open region given by the original charge source. It means using equipotential contours between the finite parallel plates as UFE profiles results in the same field distribution. Since the original parallel plates will be replaced by the generated electrode profiles in the final setup, they should be regarded as a source of virtual charge in the design process. We call them the virtual plates or virtual electrodes. For the sake of a good performance, the selected UFE profile must be an equipotential contour that well-contains the region of large fringe fields at the edges of the virtual plates, or even better cuts through a region with a monotonically decreasing field away from the central region. In contrast to the mathematical smoothness at the jointing points in the curve-joining method, the selection rule of the equipotential method is directly based on the physical distribution of the goal fields established by the virtual electrodes.

2.1. Rogowski profiles — the 2D equipotential profiles

In 1923, Rogowski first proposed to use the equipotential lines between a pair of 2D semi-infinite parallel plates as electrode profiles [1]. The 2D Laplace's equation for a pair of parallel semi-infinite plates at potentials $\pm V_0$ with a separation d is analytically solvable via conformal mapping. The coordinates of equipotential lines are expressed as

$$x = \frac{d}{\pi}(\phi + e^{\phi}\cos\psi)$$
$$y = \frac{d}{\pi}(\psi + e^{\phi}\sin\psi), \quad (1)$$

where ϕ and ψ represent different field and equipotential lines, respectively. Each equipotential line at any given value, $\psi \in (0, \pi)$, composes a UFE profile. The class of profiles was later well known as Rogowski profiles. A 3D electrode shape has to be constructed by revolving a 2D Rogowski profile around an axis in the y-direction as the best approximation. It was experimentally found that $\psi = \pi/2$ performs the best and has the simplest expression, $\psi = 2\pi/3$ might be acceptable, but $\psi = 5\pi/6$ always sparks at the edges ahead of that in the central region [2]. These results indeed reflect the selection rule of the equipotential method.

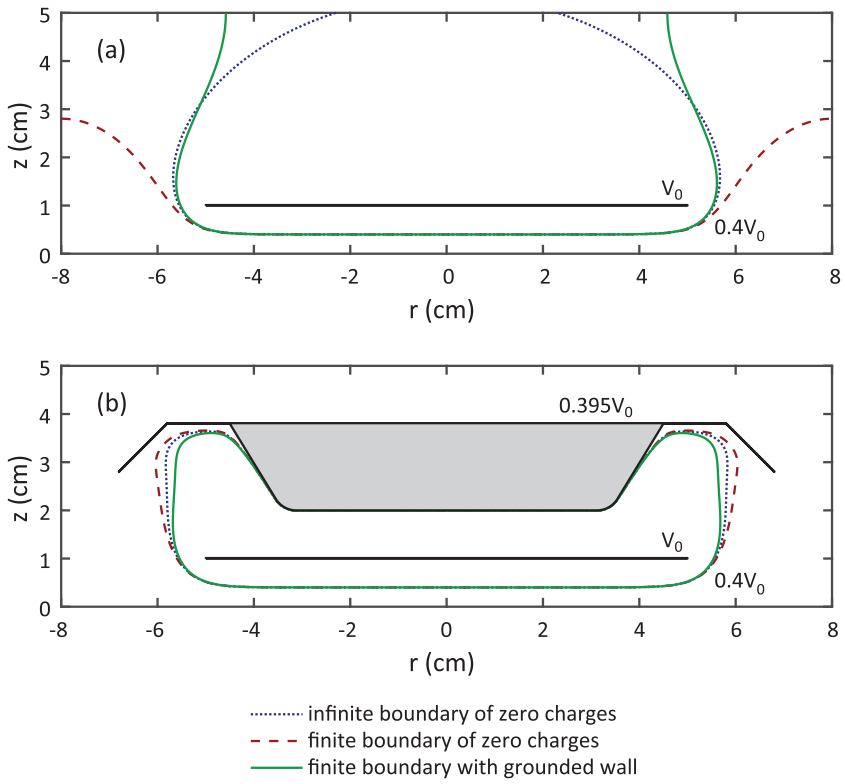

Fig. 2. The shapes of $0.4V_0$ equipotential profile are affected by different boundary conditions as shown in (a) and an additional molding electrode in the back as shown in (b). The equipotential profile with an infinite boundary approximated by a large spherical surface ($R \gg w$) with zero charges is plotted in blue dotted line; that with a finite boundary of zero charges on surfaces of a cylindrical volume, $r = 8$ cm and $z = 5$ cm are plotted in red dashed line; and that with a finite boundary of a grounded cylindrical wall at $r = 8$ cm is plotted in green solid line. (For interpretation of the references to color in this figure legend, the reader is referred to the web version of this article.)

The Rogowski profiles are apparently an expediency to use a 2D solution of Laplace's equation on a 3D problem. Harrison analyzed the performance of Rogowski profiles by simulations with finite difference method, and obtained a numerical profile by solving the 3D Laplace's equation in cylindrical coordinates. He essentially adopted the equipotential method, except enforcing the central region with a flat surface, which is a blend with curve-joining [4].

2.2. Analysis of the 3D equipotential profiles

We continue to study the 3D equipotential profiles. Shape and dimension of the virtual plates are chosen according to the goal field distribution, electrode dimensions and actual boundary conditions. For the sake of simplicity, we will generate a cylindrically symmetric UFE profile and discuss its performance. The 3D Laplace's equation reduces to quasi-2D in the coordinates of r and z.

Suppose the goal uniform field E_0 is 100 kV/cm in a cylindrical central volume of 5 cm diameter and 0.8 cm high. We may choose a pair of ultra-thin parallel virtual disk plates of 10 cm diameter at a separation of 2 cm. To fulfill the requirement of the fields, they are charged on potentials of $V^{(\pm)} = \pm V_0 = \pm 100$ kV, respectively. Once the virtual plates are set up, the field distribution in the open region is readily established. Arbitrary pair of equipotential lines may be chosen as electrode profiles, but the spatial distribution of fields has been fixed relative to the virtual plates. Since the equipotential lines are evenly spaced in the central region of uniform fields, the z-coordinate of the αV_0 equipotential line can be expressed as $z = \alpha d/2$, where α is the fraction of the set potential on the virtual plate. As the desired separation between the generated electrodes is 0.8 cm, the equipotential lines of $\pm 0.4V_0$ immediately become the choice for the symmetric electrode profiles. Besides, the electrode pair may also be asymmetric, e.g. equipotential lines of $+0.5V_0$ and $-0.3V_0$ can give the same uniform field of 100 kV/cm at a separation of 0.8 cm. This asymmetric pair may become appealing when the power cable in the negative polarity is vulnerable against partial discharges at high voltages.

We may further look into the properties of different equipotential lines given in the example above. As shown in Fig. 1a, equipotential lines of $V = V_0/6$, $V_0/3$, $V_0/2$, $2V_0/3$, $5V_0/6$ are plotted in red solid lines on top of the field distribution established by the virtual plates at $\pm V_0$. Apparently, the $5V_0/6$ profile is inappropriate and the $2V_0/3$ profile is marginal, because the high fringe fields will remain outside of the generated electrodes. Fig. 1b shows the field discrepancy defined by $|\Delta E|/E_0$ in solid contours of 0.1%, 0.2%, 0.5%, 1%, 2% and 5%. Along the middle plane, the field discrepancy exceeds 0.1% and 1% at radii of about 3.0 cm and 3.8 cm, respectively. There are two groups of discrepancy contours: the upper group of positive discrepancies represents the fields larger than E_0, whereas the lower group of negative discrepancies represents the fields smaller than E_0. If a positive discrepancy of 5% is allowed on the generated electrode surface, the equipotential profile of $0.56V_0$ that crosses the upper group could become an option. See the orange dotted line in Fig. 1b. For most UFE profiles, however, it is preferred that the fields on the surface monotonically decrease away from the region of uniform fields. Therefore, the chosen equipotential profile should cut across the lower group of the negative discrepancies. The separation line that begins to meet this criterion is the $V_0/2$ equipotential profile as plotted in Fig. 1b in red solid line. The surface fields decrease rapidly from E_0 in a small radial distance on the edge of the $V_0/2$ equipotential profile. In addition, for a given goal electrode separation d_1, $V_0/2$ equipotential profile originates from virtual plates with a separation $d = 2d_1$. Being the smallest separation among profiles of $\alpha \leqslant 1/2$, it results in the largest width-to-separation ratio (w/d) of the virtual plates, and hence the best field distribution. This is why the $V_0/2$ equipotential profile is the most popular option in practice.

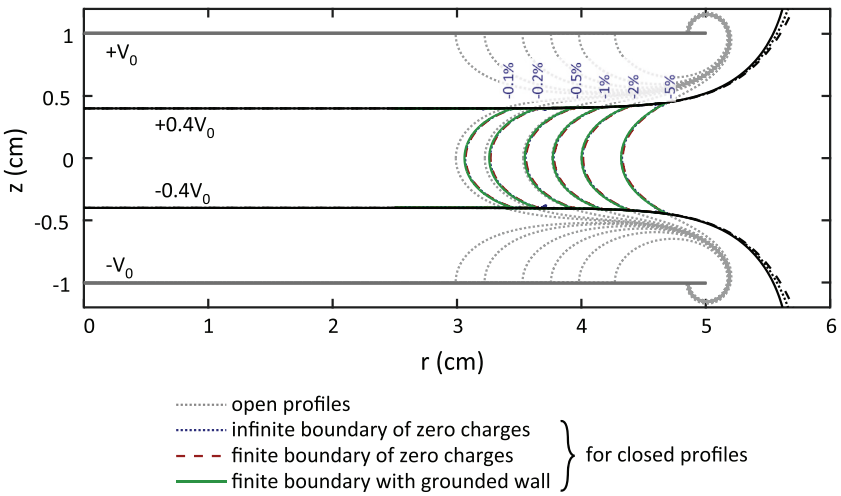

Fig. 3. Discrepancy contours of the $0.4V_0$ closed profiles are plotted for different boundary conditions. The equipotential profile and its corresponding discrepancy contour with an infinite boundary approximated by a large spherical surface ($R \gg w$) with zero charges are plotted in black and blue dotted lines, respectively; those with a finite boundary of zero charges on surfaces of a cylindrical volume, $r = 8$ cm and $z = \pm 5$ cm are plotted in black and red dashed lines, respectively; and those with a finite boundary of a grounded cylindrical wall at $r = 8$ cm are plotted in black and green solid lines, respectively. As a comparison, the discrepancy contours for open profiles, equivalent to that of the virtual parallel plates, are plotted in gray dotted line. The differences in field uniformity among the closed profiles of different boundary conditions are negligible, but it is obvious between the open and closed profiles. (For interpretation of the references to color in this figure legend, the reader is referred to the web version of this article.)

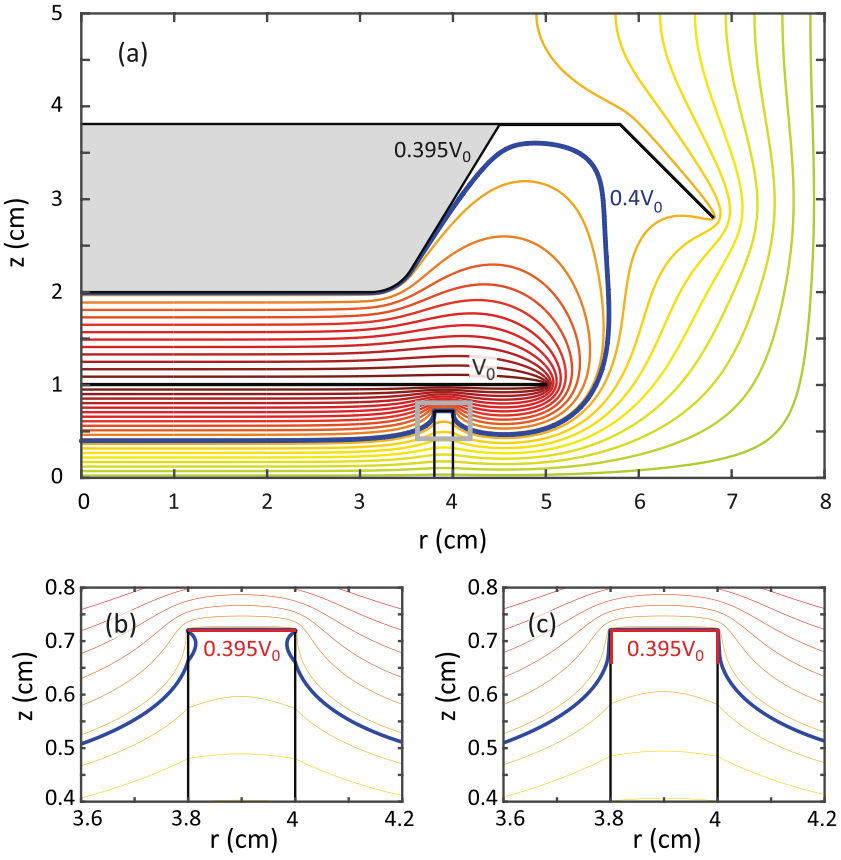

Fig. 4. (a) Generation of the closed and recessed profile for an annular dielectric cylinder with equipotential method. (b) A highlight in the region where the end surface of the dielectric is set as a virtual molding electrode at $0.395V_0$ to form the recess, but the equipotential lines bend into the dielectric. (c) Short vertical molding electrodes are added to fully repel the equipotential line out of the given dielectric. The virtual molding electrodes in (b) and (c) are marked in red solid lines. (For interpretation of the references to color in this figure legend, the reader is referred to the web version of this article.)

Nevertheless, the $0.4V_0$ equipotential line as taken in the example satisfies all the criteria, though it is not the best.

As a comparison, the Rogowski profiles of $\psi = \pi/6$, $\pi/3$, $\pi/2$, $2\pi/3$, $5\pi/6$ are also plotted in Fig. 1a in green dotted lines. The differences between the Rogowski and 3D equipotential profiles are dramatic outside the region of uniform fields. The field discrepancies $|\Delta E|/E_0$ of 0.1%, 0.2%, 0.5%, 1%, 2% and 5% for the $\pi/2$ Rogowski profile are also plotted in Fig. 1b in green dashed lines. We find that the uniform field region of the 3D equipotential profiles is smaller than that of the $\pi/2$ Rogowski profile, but it does not mean our method is in general

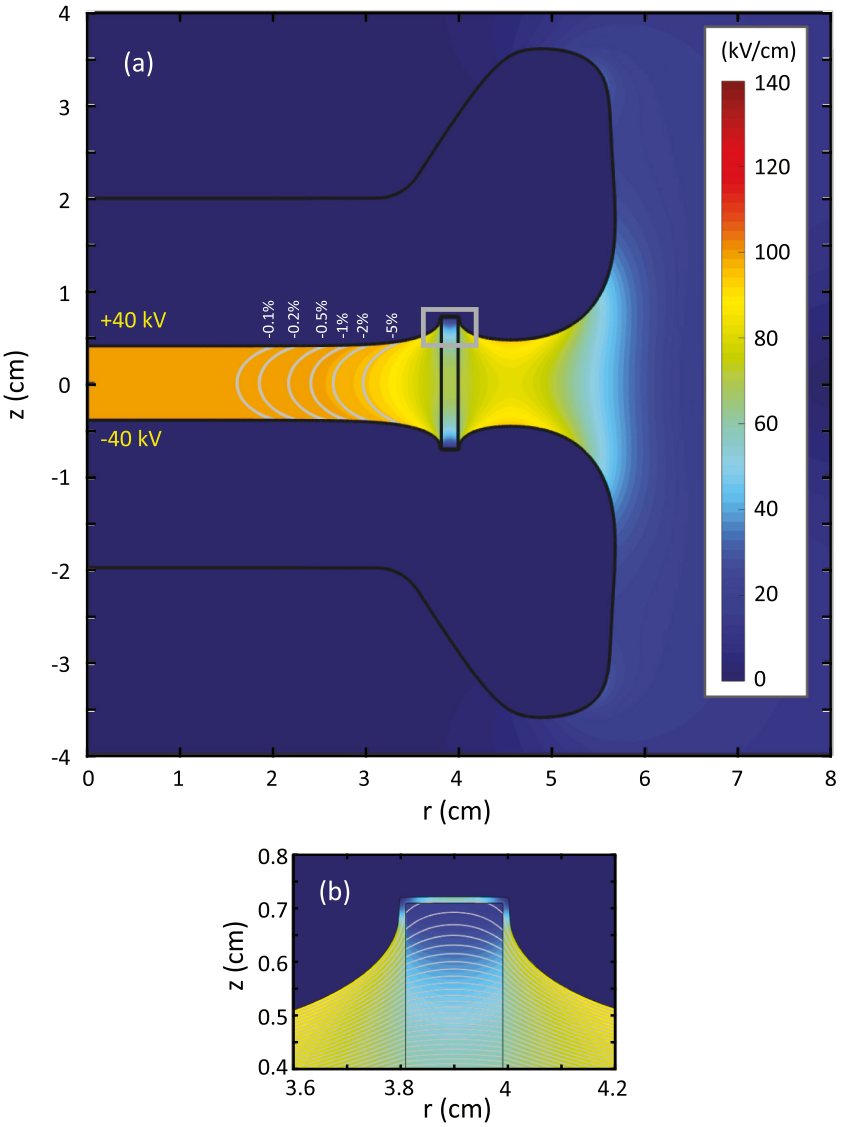

Fig. 5. Results of the test simulation with ±40 kV applied on the generated recessed profiles for the annular dielectric cylinder. The field distribution and contours of −0.1%, −0.2%, −0.5%, −1%, −2% and −5% field discrepancies are plotted in (a), and the highlight in the electrode recess is shown in (b). (For interpretation of the references to color in this figure legend, the reader is referred to the web version of this article.)

inferior to the Rogowski profile. In fact, it is due to the small width-to-separation ratio ($w/d = 5$) of the virtual plates used in this example. Further study shows w/d ratios of the virtual plates needs to exceed 40 for the 3D equipotential profiles to perform better. More interestingly, the virtual electrodes for generation of UFE do not necessarily have to be parallel plates, but could also be the Rogowski profile. For instance, the $\psi = 5\pi/6$ Rogowski profile with its edge properly truncated can be positioned at $z = \pm 5d/12$ and set on potential of $\pm 5V_0/6$ to replace the parallel virtual plates.

Moreover, boundary conditions also impact the shape of the equipotential profiles. As shown in Fig. 2a, we look into three different boundary conditions and compare the resultant $0.4V_0$ equipotential profiles. (i). With an infinite boundary, which is approximated by a large spherical surface ($R \gg w$) with zero charges, the $0.4V_0$ equipotential line tends to close the loop behind the virtual plate. (ii). With a finite boundary of zero charges on surfaces of a cylindrical volume, at $r = 8$ cm and $z = \pm 5$ cm, the $0.4V_0$ equipotential line is attracted towards the boundary cylindrical surface of $r = 8$ cm, as the equipotential lines always end up perpendicular to the boundaries of zero charges. (iii). With a finite boundary of a grounded cylindrical wall at $r = 8$ cm, the $0.4V_0$ equipotential line is squeezed by the grounded wall and terminates at the upper and lower boundaries of zero charges at $z = \pm 5$ cm.

2.3. Generation of closed 3D UFE profiles

As we may see in Fig. 2a, many equipotential contours are open surfaces due to the boundary conditions. However, it must be a closed surface to become a compact electrode, and often, its back is required to be of some special shape to accommodate structural support and electrical connection. In 1985, Girdinio et al. used the equipotential method and created a complete electrode profile with a straight cylindrical back [10]. By the guidance of a thin virtual metal stem behind the virtual plate electrode, the equipotential profile was gradually bent into a straight cylindrical surface in the back. Recently, Davidson took advantage of the grounded walls of the test chamber and produced a droplet-shaped electrode with the equipotential method, though it was named differently as the Rogowski method [24]. In the following, we will introduce a new approach to generate a concave electrode back with a flat central region for structural mounting. By analogy with the shaping technique in fabrication of ceramic or metal objects, we call it the molding technique on shaping equipotential profiles.

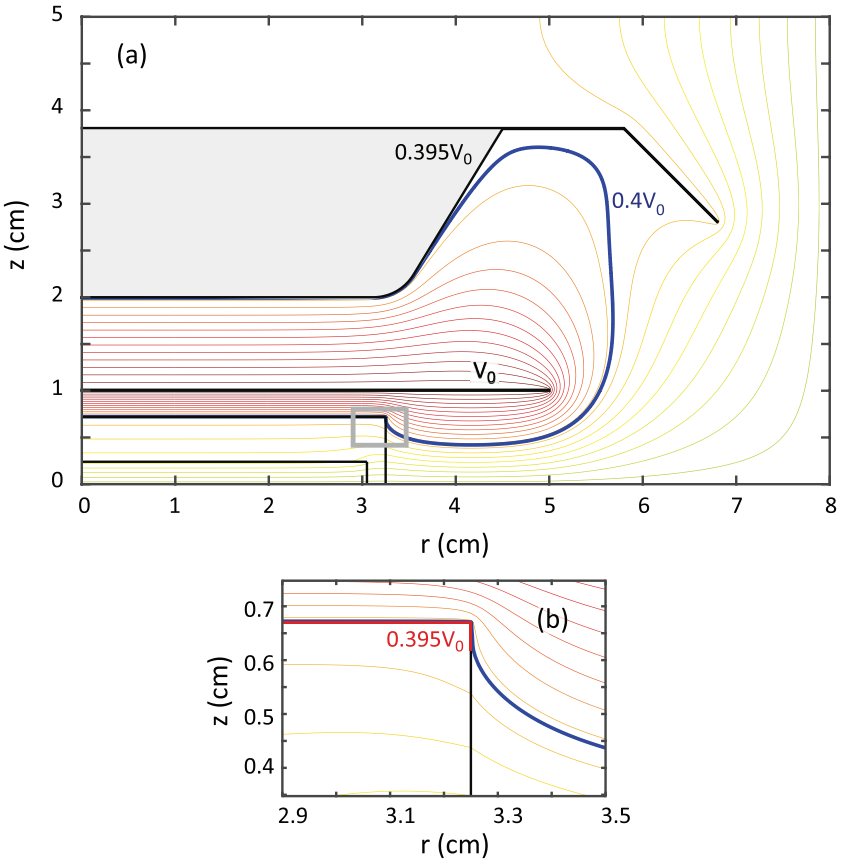

Fig. 6. (a) Generation of the closed and recessed profile for a closed cylindrical dielectric cell with equipotential method. The region within the lines $z = 0.24$ cm and $r = 3.05$ cm is the inner volume of the cell. (b) A highlight in the region where the end surface and a short section of the side surface on the dielectric are set as virtual molding electrodes at $0.395V_0$ to form the recess. The virtual molding electrodes in (b) are marked in red solid lines. (For interpretation of the references to color in this figure legend, the reader is referred to the web version of this article.)

An additional set of molding electrodes is employed to deform the equipotential profile into a desired shape. They are defined as conductors on a potential slightly less than that of the target equipotential contour, so that they will always stay outside of the closed contour. Nevertheless, such a molding technique is semi-physical, as the inserted molding electrodes intercept the back of the generated profile from the actual boundary conditions. Therefore, it cannot guarantee the performance of the resultant electrode profile. Once a design finishes, all the molding electrodes will be removed. A stand-alone test on the generated electrode profile must be passed in the actual environment. Some trial-and-errors are needed to achieve a satisfactory result. Since none of the molding electrodes will remain in the final setup, they are henceforth called virtual molding electrode or virtual mold, and all the fields terminating on them are called the virtual fields.

As an example, we continue to work on the $0.4V_0$ electrode profile obtained in Section 2.2, and modify its back into a concave shape. The virtual mold is set up as shown in Fig. 2b. Its cross section looks like a bird with a wide body but short spreading wings. Its potential is set at $0.395V_0$, or any other value slightly less than $0.4V_0$ of the target equipotential line, so that the mold will always stay outside of the closed electrode profile. A region of low virtual field is formed underneath the wings of the mold, and boldly bends the equipotential profile outside the parallel virtual plates to form a closed loop. Meanwhile, a region of high virtual field resides along the protruding bottom of the mold, and pull the equipotential profile tightly against the shape of the bottom. Unfortunately, the shape of the virtual mold, particularly its spreading wings, is constructed heuristically. It benefits from a good understanding on distributions of field lines and equipotential contours in a wedge corner of arbitrary angle formed by two conductive planes. A 2D analytical solution to this problem is presented in detail in Jackson [25]. Intuitively, obtuse angles plus a proper length of the wings define a low local virtual field and assist the equipotential profile to bend in large curvature; whereas, shapes protruding towards the main virtual plate carry high surface virtual field, and hold the equipotential profile tightly against itself. After the design finishes, a stand-alone test without the virtual mold has verified that the profile of electrode back produces no high local field as shown in Fig. 5 or Fig. 7.

In addition, Fig. 2b also shows how different boundary conditions impact the side and back of the electrode shape. The profile generated with a grounded cylindrical wall appears to be the most compact. Fig. 3 shows the differences in field uniformity are negligible among the three closed profiles in different boundary conditions, yet their region of uniform field slightly enlarges compared to the open profiles, especially at the discrepancy levels of -0.1% and -0.2%. Therefore, both the virtual molds and boundary conditions have some mild impact on the shape of the electrode profile and the field distribution in the target region.

3. Generate electrode profiles with a recess to accommodate dielectric objects

Placing a dielectric object in high electric fields is always challenging in electrode design. It is known that a dielectric surface flashover usually initiates in the triple junction region of cathode, dielectric and vacuum/ambient medium. A review by Miller summarized how to improve the maximum holding voltages by variation of dielectric parameters, such as material, geometry, surface finish and conditioning, *etc* [26]. Pallai and Hackam analyzed and compared three different types of electrode profiles that sandwich a dielectric bulk: (i) planar

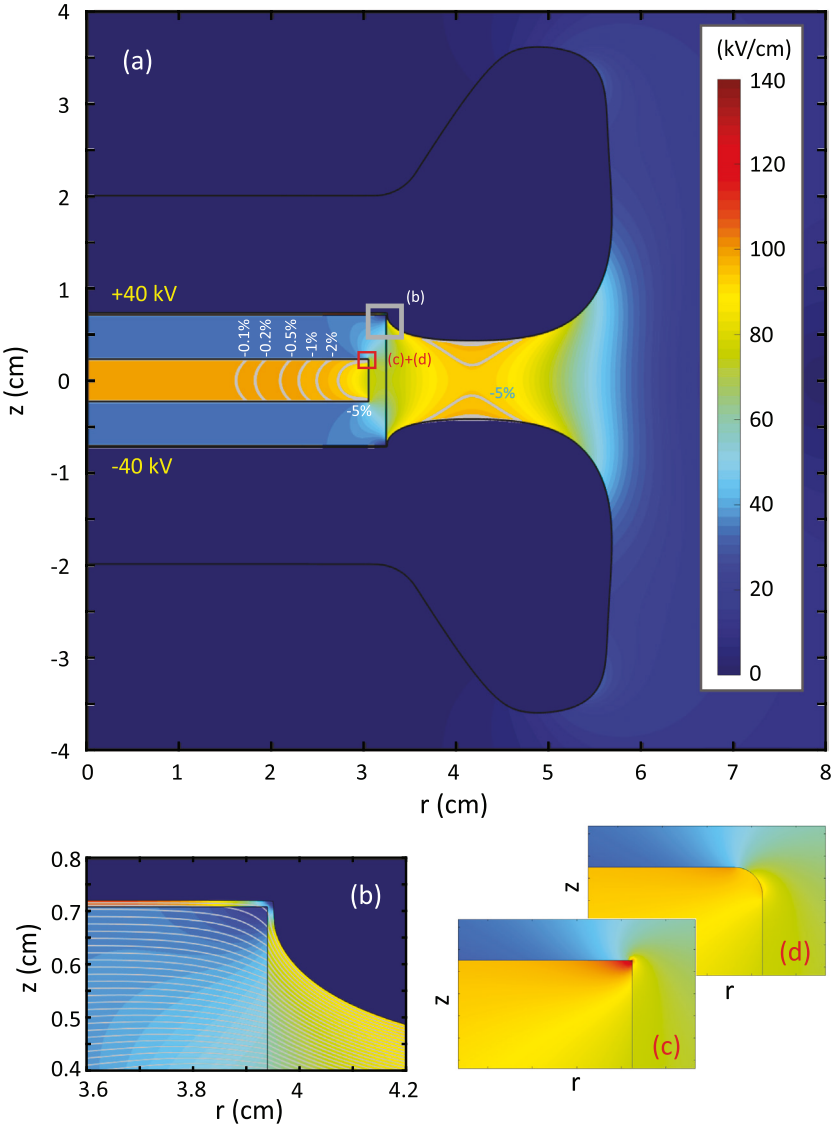

Fig. 7. Results of the test simulation with ±40 kV applied on the generated recessed profiles for the closed cylindrical dielectric cell. The field distribution and contours of −0.1%, −0.2%, −0.5%, −1%, −2% and −5% field discrepancies are plotted in (a), (b) highlights the corner of electrode recess, (c) shows a singularity point formed by square dielectric corner in simulation, but it can be removed by rounding the corner as in (d). (For interpretation of the references to color in this figure legend, the reader is referred to the web version of this article.)

electrodes attached to the dielectric, (ii) electrodes with an extrusion inserted in the dielectric, and (iii) electrodes with a recess to seat the dielectric [21,27]. In types (i) and (ii), a void-free contact between the surfaces of electrode and dielectric is crucial to avoid breakdown. Similarly, the dielectric bulk must be void-free to avoid partial discharge [28]. Besides, surface charging on dielectrics also plays an important role in the performance of maximum holding voltages. For example, chamfers at the dielectric corner of the triple junction in type (i) in general induce a high local field and lower the maximum holding voltage. However, Jaitly and Sudarshan showed that electrons can accumulate on the surface of the chamfer on the cathode side, relieve the local stress, and improve the maximum holding voltage. [29] Nevertheless, in this paper, we will not consider the variation of dielectric properties, but focus on the design method of a recessed electrode as of type (iii) without surface charges. We may see the merit of recessed electrodes is to allow a small spacing between the surfaces of electrode and dielectric, *i.e.* the dielectric structures are not bonded to the electrodes and are replaceable with the electrodes intact. The boundary conditions at the interface of different dielectric materials are $\epsilon_1 E_{n1} = \epsilon_2 E_{n2}$ for no surface charges in the normal direction, and $E_{t1} = E_{t2}$ in the tangential direction. Hence, a dielectric interface refracts electric fields. The higher the ratio of dielectric constants $\epsilon_r = \epsilon_1/\epsilon_2 > 1$, the larger a refraction of fields. This complicates the manipulation of the equipotential lines. In the following examples, we take the relative permittivity of the dielectric as $\epsilon_r = 3$, a median value in common plastics, and that of the free space as unity.

In this section we will employ the equipotential method to generate recessed electrode profiles for three dielectric geometries, (a) an annular cylinder, (b) a cylindrical closed cell, and (c) a cuboidal closed cell in Sections 3.1, 3.2 and 3.3, respectively. Each of the dielectric geometries is for a specific and independent application in different circumstances. Since we are pursuing a near-UFE profile despite the existence of dielectric structures, parallel virtual plates are still the best option to provide the basis of a uniform field. A variation of the molding technique will be used to create a recess on the electrode front. In Sections 3.1 and 3.2 we may directly work out the corresponding recessed profiles for dielectric geometries (a) and (b) on top of the closed electrode profile generated in Section 2.3. The goal uniform field is still $E_0 = 100$ kV/cm with a boundary condition of a grounded cylindrical wall at $r = 8$ cm. In Section 3.3 we present a 3D case of

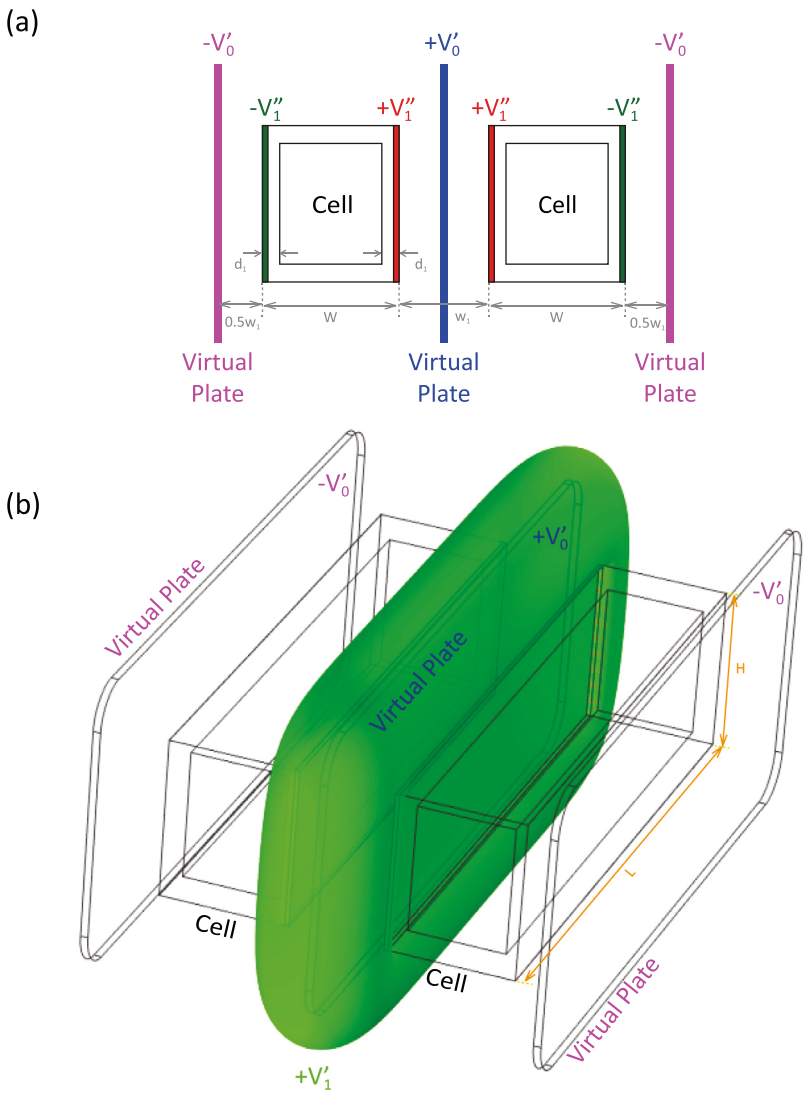

Fig. 8. (a) Schematics on the configuration of the virtual plates to generate a recessed profile that can accommodate a pair of closed cuboidal dielectric cells with equipotential method. (b) The $+V_1'$ equipotential contour highlighted in light green is the generated recessed profile for the HV electrode. The relationship between the set potentials are $V_1' = 0.332V_0'$, and $V_1'' = V_1' - \delta V$, where $\delta V \ll V_1'$. (For interpretation of the references to color in this figure legend, the reader is referred to the web version of this article.)

lower symmetry with a cuboidal closed cell to further demonstrate the merit of the equipotential method.

3.1. A recessed profile for an annular dielectric cylinder

Suppose an annular dielectric cylinder is about 4 cm in outer radius, 0.2 cm thick and 1.4 cm high. We want a profile with a groove-like recess to protect the annular cylinder. In order to push the $0.4V_0$ equipotential line out of the dielectric bulk, the end surface of the annular cylinder is set as a virtual molding electrode at $0.395V_0$, which is slightly less than that of the equipotential profile. The front profile deforms into a groove with smooth transitions as shown in Fig. 4a. But if zooming into the recess region as shown in Fig. 4b, it is found that the $0.4V_0$ equipotential profile bends into the dielectric due to the refraction of fields. Such an electrode profile is the most natural given by the equipotential method. However, it asks for complicated machining and the seamless bonding — impractical to fabricate. In order to push the equipotential line fully out of the given dielectric, short vertical virtual molding electrodes at $0.395V_0$, as shown in red solid lines in Fig. 4c, are added on both the inner and outer walls. The height is chosen as approximately up to the previous intersection point of the equipotential line on the dielectric surfaces. The resultant $0.4V_0$ equipotential profile then bends away from the dielectric and forms a clean groove.

The field distribution with ±40 kV applied on the generated electrode profiles is shown in Fig. 5a, with contours of −0.1%, −0.2%, −0.5%, −1%, −2% and −5% field discrepancies. The dielectric object in the test simulation is shrunk slightly for clearance to allow easy assembling in practice, and all of the virtual electrodes are removed. As shown in Fig. 5b, the field is in good uniformity in the central region; yet in the vicinity of the annular dielectric cylinder, the discrepancy is as high as 30% on the middle plane, and up to 37% close to the recess, due to existence of the dielectric object. Along the recess profile, the field variation is smooth, and most importantly, free of local hot spots. In the context of equipotential method, it may be physically interpreted as no stray virtual charges inside the electrode profile other than those unevenly distributed on the parallel virtual plates. In the recess, dielectric stays in low fields as expected. The depth of the recess is about 1.6 times the wall thickness in this example. A deeper recess is needed to accommodate a thicker annular cylinder in satisfactorily low fields. This inevitably induces larger non-uniformity near the dielectric. Therefore, the thickness of the annular cylinder should be minimized to the limit of the mechanical requirement in engineering.

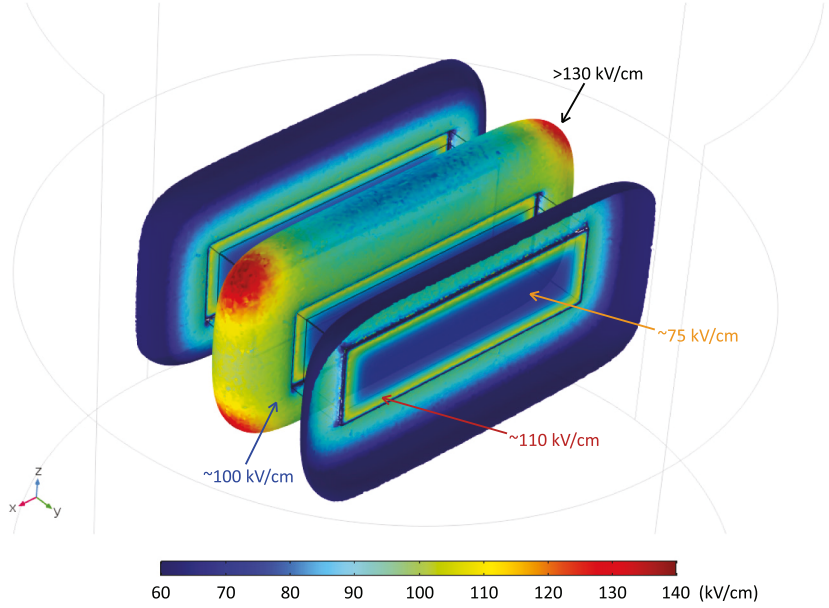

Fig. 9. Results of the test simulation — the field distribution on the surfaces of the recessed electrode profile for a pair of closed cuboidal dielectric cells. The central HV electrode is set at 635 kV, and two side electrodes are grounded. (For interpretation of the references to color in this figure legend, the reader is referred to the web version of this article.)

3.2. A recessed profile for a closed cylindrical dielectric cell

Suppose a closed cylindrical dielectric cell is about 3.24 cm in outer radius and 1.44 cm high. Compared with the annular cylinder, the closed cell has two large end disks. We will again modify the front of the $0.4V_0$ equipotential UFE profile obtained in Section 2.3 into a wide recess to hold the closed cell. In order to get the goal uniform field $E_0 = 100$ kV/cm, the thickness of the end disks d_1 and the inner height of cell d_2 can be easily calculated via $0.8V_0 = E_0(2d_1/\epsilon_r + d_2)$. As a result, both d_1 and d_2 are 0.48 cm, given the dielectric constant $\epsilon_r = 3$. Similar to what has been done in Section 3.1, the end surfaces of the cell and additional short vertical sections on the outer wall are set as virtual molding electrodes on a potential of $0.395V_0$, slightly lower than $0.4V_0$ of the equipotential profile. Fig. 6a shows a recess is generated on the front of the equipotential profile. Fig. 6b shows the local profile in the vicinity of the recess smoothly bends away from the dielectric wall, owing to the short vertical virtual molding electrodes.

Apparently, the thickness of the cell side wall has little impact on the shape of the recessed electrode profile in the molding process, but its effect on the final field distribution along the recessed electrode surface can be significant. In a test simulation, a closed cell slightly shrunken in size is placed together with the generated profile, and all of the virtual molding electrodes are removed. Fig. 7a shows the field distribution with ±40 kV applied voltages, and contours of the −0.1%, −0.2%, −0.5%, −1%, −2% and −5% field discrepancies. Fig. 7b shows the field is in good uniformity in the central region, yet the discrepancy is as high as 23% in the middle plane close to the wall of the cell. There is a spot of high fields at the inner corner of the dielectric cell as highlighted in Fig. 7c. It is due to the singularity of electric fields at the concave corner of an dielectric object [30], but can be removed by a rounding as shown in Fig. 7d. The same phenomenon has been observed by Chiou et al. in dielectric wave guide simulations [31]. As shown in Fig. 7b, the edge of the cell stays in low fields of the recess. With the cylindrical cell wall of about 0.2 cm thick, the field in the small spacing between the cell and electrode monotonically increases to a uniform high field in the central region. However, studies have shown a local region of high fields might appear in the small spacing for a thick cell side wall. It can be problematic and initiate local breakdown. In this case, the depth of the recess has to be increased for an improvement.

In fact, the field distribution inside the closed cell is no longer set by the parallel virtual plates as in the case of the annular cylinder. The role is taken over by the virtual molding electrodes on the cell end surfaces. The original parallel virtual plates turn to control the depth of the wide recess, and determine the field strength on the fringe lobe of the generated profile. The recess can be deepened by increasing the potential difference between the original parallel plates while holding the value of the equipotential line fixed, which is equivalent to lowering the α value of the chosen equipotential profile. The downside of this operation is that the maximum field on the lobe will be increased. It could be much higher than the fields in the cell, but not exceed the mean value of fields given solely by the virtual plates. This could be used as a quick estimate of the upper limit of field strength on the fringe lobe in complex problems before spending a long computing time. It reflects a merit of the equipotential method. We will see more in the following subsection.

3.3. A recessed profile for a closed cuboidal dielectric cell

In the last example, the equipotential method will be applied to a recessed profile to accommodate a dielectric object of lower symmetry — a cuboidal closed cell. Here, we work on a special configuration of two identical cuboidal cells clamped onto a high voltage electrode by two ground electrodes from opposite sides, as shown in Fig. 8. Outer dimensions of the cells are $L \times H \times W$ ($L \gg H, W$), and the thickness of the cell wall is d_1 for all the six sides. The closest surfaces between the two cells are w_1 apart. The goal electric fields in the two cells are E_0 in opposite directions, *i.e.* the HV electrode will be charged to a potential of $V_1 = E_0 \times [W - 2d_1(1 - 1/\epsilon_r)]$, where dielectric constant is set as $\epsilon_r = 3$. The boundary condition is a grounded cylindrical wall of D in diameter, which is slightly larger than $2L$.

As a demonstration of the equipotential method, we will only generate a profile for the HV electrode, and use it as the ground electrodes in the test simulation. This approximation will lead to small deviations because of the lower symmetry in the overall geometry. As shown in Fig. 8a, the virtual electrodes are set up similar to what is done in Section 3.2, but including (i) 3 rectangular virtual parallel plates, one for the central HV electrode highlighted in blue, and two for the side ground electrodes in magenta, (ii) a total of 4 cell outer surfaces that will be in contact with the generated electrode profiles, and (iii) a total of 16 short up-standing sides in junction with each of the former cell outer surfaces to expel equipotential lines out of the

cell wall, where items (ii) and (iii) are the virtual molding electrodes illustrated in dark green and red, respectively. There are two different ways of assigning preset potentials on the virtual electrodes. If directly working on the V_1 equipotential profile, the virtual molding electrodes on the cell outer surfaces should be set at $V_1 - \delta V$ and δV, respectively, where $\delta V \ll V_1$. Some simple calculations will give the preset values of the three rectangular virtual plates. However, in this case study, we take an alternative way to set the potentials on the virtual HV and ground electrodes symmetric in positive and negative polarities. This will result in some minor distortions in the final field distribution, because the grounded volume wall, $\Phi|_{r_{wall}} = 0$, is a first-type boundary condition that is not compatible with shifting of potential values in Laplace's equation. Studies suggest the distortions mostly occur in the edge region and become insignificant in the central region. In such a scenario, we will work on the equipotential profiles of $V_1'^{(\pm)} = \pm V_1' = \pm V_1/2$; the virtual molding electrodes on the cell outer surfaces are set as $V_1''^{(\pm)} = \pm V_1'' = \pm(V_1' - \delta V)$; and the three rectangular virtual parallel plates are set as $\pm V_0'$, where $V_1' = 0.332 V_0'$, to deform the equipotential profiles into a recess and accommodate the cuboidal cell. Because the ratio $\alpha = V_1'/V_0'$ is equal to 0.332, much smaller than 0.5, the generated equipotential contour should be able to well contain the high fringe fields of the virtual parallel plates, and the maximum field on the lobes should be less than the mean field E_0' solely given by the pair of virtual parallel plates at $\pm V_0'$,

$$E_{lobe}^{(max)} \leqslant E_0' = \frac{2V_0'}{W + w_1} = \frac{E_0}{0.332} \frac{W - 2d_1(1 - 1/\epsilon_r)}{W + w_1}. \quad (2)$$

The configuration of virtual electrodes, as well as the generated 3D HV electrode profile, are shown in Fig. 8a and b, respectively. The profile looks like a pillow with a recess surrounded by smooth lobes. A test simulation is performed with the central HV electrode at $V_1 = +635$ kV and two side electrodes grounded. The surface field distribution is plotted in Fig. 9. The edges of the dielectric cell sit in low fields formed by the L-shaped sides of the recess. But a rectangular band of high fields at a maximum of about 110 kV/cm appear on the recessed surface aligning with the cell side walls because of the large wall thickness d_1. Most of the recessed surface carries a field close to $E_0 = 75$ kV/cm, which is the design goal of the field strength in the cell inner volume. The maximum field on the lobes is about 100 kV/cm, which agrees with the estimation given by Eq. (2). The highest fields of more than 130 kV/cm appear on the four corners on the generated HV electrode, even though the rectangular virtual plates have been rounded. This is due to stacking of curvatures in two orthogonal directions. Some scattered spots of local high fields seem to reach up to about 140 kV/cm, but it could come from the coarse mesh used in this simulation. There is still room to improve, but further optimization will not be presented, as this paper only focuses on demonstration of the equipotential method.

4. Conclusion

In this paper, we have presented the equipotential method, expanded it into a new approach of generating smooth and closed electrode profiles by manipulation of the equipotential contours, and further demonstrated designs of recessed electrodes to accommodate dielectric structures of various geometries with the molding technique. As a summary of the equipotential method, the goal field in the region of interest is first constructed by a set of virtual electrodes according to the physics of electrostatics, and then the associated equipotential contours immediately become options of an electrode profile with the field distribution along the electrode surface known *a priori*. Many parameters are available for fine-tuning the shape of the generated electrode profile, such as the preset dimensions and potentials of the virtual electrodes, boundary conditions, *etc.* As introduced in Section 2.3 and used in the three examples of Section 3, the molding technique is a semi-physical approach to modify the shapes of equipotential profiles. The greatest advantage of the equipotential method is in generating 3D electrode profiles of low symmetry or irregular shapes. It has the potential to offer satisfactory solutions to complex 3D problems. Since the nature of virtual electrodes is to deploy a distribution of virtual charges so as to establish the goal fields in the region of interest, future studies may also investigate how to improve the field distribution and associated equipotential electrode profile by redistributing the charges on the virtual electrodes. Nevertheless, we have to acknowledge the existence of many technical issues, such as file format compatibility, mesh refining, *etc.*, in transition from the 3D modeling programs to the manufacturing control software. But as new technologies in 3D animation and 3D printing develop and prevail, more industrial tools are emerging in the market. Hopefully, its versatility and flexibility will make the equipotential method more and more popular in the electrode designs for complex problems in various applications.

Declaration of competing interest

The authors declare that they have no known competing financial interests or personal relationships that could have appeared to influence the work reported in this paper.

Acknowledgments

The author thanks R. Carr, V. Cianciolo, S. Clayton, R. Golub, M. Hayden, T. Ito, S. Lamoreaux, R. Pattie, J. Ramsey, C. Swank and Z. Tang for helpful comments and discussions. This work was supported by the US Department of Energy under Contract No. DE-AC52-06NA25396 under proposal number LANLEEDM and the National Science Foundation, USA under Grant No. 1812340.

References

[1] W. Rogowski, Die elektrische festigkeit am rande des plaltenkondensators: Ein beitrag zur theorie der funkenstrecken und Durchführungen, Arch. Elektrotech. 12 (1923) 1–15.
[2] J.D. Cobine, Gaseous Conductors: Theory and Engineering Applications, Dover, 1958, sec.7.12 Ideal Plane Electrodes.
[3] F.M. Bruce, Calibration of uniform-field spark-gaps for high-voltage measurement at power frequencies, J. Inst. Electr. Eng. 94 (1947) 138–149, http://dx.doi.org/10.1049/ji-2.1947.0052.
[4] J.A. Harrison, A computer study of uniform-field electrodes, Br. J. Appl. Phys. 18 (1967) 1617–1627, http://dx.doi.org/10.1088/0508-3443/18/11/316.
[5] J.S. Pearson, J.A. Harrison, A uniform field electrode for use in a discharge chamber of restricted size: design and performance, J. Phys. D: Appl. Phys. 2 (1969) 77–84, http://dx.doi.org/10.1088/0022-3727/2/1/312.
[6] J.A. Harrison, The electric field on the surface of Bruce electrodes, J. Electrost. 2 (1977) 327–330, http://dx.doi.org/10.1016/0304-3886(77)90003-1.
[7] T.Y. Chang, Improved uniform-field electrode profiles for tea laser and high-voltage applications, Rev. Sci. Instrum. 44 (1973) 405–407, http://dx.doi.org/10.1063/1.1686144.
[8] G.J. Ernst, Compact uniform field electrode profiles, Opt. Commun. 47 (1983) 47–51, http://dx.doi.org/10.1016/0030-4018(83)90334-6.
[9] G.J. Ernst, Uniform-field electrodes with minimum width, Opt. Commun. 49 (1984) 275–277, http://dx.doi.org/10.1016/0030-4018(84)90190-1.
[10] P. Girdinio, G. Liberti, P. Molfino, G. Molinari, A. Viviani, A new class of uniform-field electrodes for dielectric strength tests in liquids, IEEE Trans. Electr. Insul. 20 (1985) 309–314, http://dx.doi.org/10.1109/TEI.1985.348836.
[11] J. Liu, E.M. Freeman, X. Yang, J. Sheng, Optimization of electrode shape using the boundary element method, IEEE Trans. Magn. 26 (1990) 2184–2186, http://dx.doi.org/10.1109/20.104663.
[12] D.H. Kim, I.H. Park, M.C. Shin, J.K. Sykulski, Generalized continuum sensitivity formula for optimum design of electrode and dielectric contours, IEEE Trans. Magn. 39 (2003) 1281–1284, http://dx.doi.org/10.1109/TMAG.2003.810213.
[13] B. Rebel, C. Hall (Eds.), Workshop Note on Challenges of using High Voltage in Noble Liquids, 2014, arXiv:1403.3613.
[14] T.M. Ito, et al., An apparatus for studying electrical breakdown in liquid helium at 0.4 K and testing electrode materials for the neutron electric dipole moment experiment at the spallation neutron source, Rev. Sci. Instrum. 87 (2016) 045113, http://dx.doi.org/10.1063/1.4946896.
[15] L. Tvrznikova, E.P. Bernard, S. Kravitz, K. O'Sullivan, G. Richardson, Q. Riffard, W.L. Waldron, J. Watson, D.N. McKinsey, Direct comparison of high voltage breakdown measurements in liquid argon and liquid xenon, J. Instrum. 14 (2019) P12018, http://dx.doi.org/10.1088/1748-0221/14/12/P12018.

[16] S. Knapen, T. Lin, K.M. Zurek, Light dark matter in superfluid helium: detection with multi-excitation production, Phys. Rev. D 95 (2017) 056019, http://dx.doi.org/10.1103/PhysRevD.95.056019.
[17] E. Aprile, et al., The XENON100 dark matter experiment, Astropart. Phys. 35 (2012) 573–590, http://dx.doi.org/10.1016/j.astropartphys.2012.01.003.
[18] R. Golub, Model high-voltage system for apparatus to search for the electric dipole moment of the neutron with the aid of ultracold neutrons, Sov. Phys. Tech. Phys. 31 (1986) 945.
[19] A.P. Serebrov, et al., New search for the neutron electric dipole moment with ultracold neutrons at ILL, Phys. Rev. C 92 (2015) 055501, http://dx.doi.org/10.1103/PhysRevC.92.055501.
[20] M.W. Ahmed, et al., A new cryogenic apparatus to search for the neutron electric dipole moment, J. Instrum. 14 (2019) P11017, http://dx.doi.org/10.1088/1748-0221/14/11/P11017.
[21] M.J. Kofoid, Effect of metal–dielectric junction phenomena on high-voltage breakdown over insulators in vacuum, Trans. Amer. Inst. Electr. Eng. 79 (1960) 999–1004.
[22] K. Itaka, G. Ikeda, Dielectric characteristics of compressed gas insulated cables, IEEE Trans. Power Appar. Syst. 90 (1970) 1986–1994.
[23] C.M. Cooke, J.G. Trump, Post-type support spacers for compressed gas-insulated cables, IEEE Trans. Power Appar. Syst. 92 (1973) 1441–1447.
[24] A.J. Davidson, High Voltage Breakdown in the Ramsey Cell of the CryoEDM Experiment: An Experimental Study of Some Relevant Parameters (Ph.D. thesis), University of Sussex, 2011.
[25] J.D. Jackson, Classic Electrodynamics, Wiley, 1999, sec.2.11 Fields and charge densities in two-dimensional corners and along edges.
[26] H.C. Miller, Flashover of insulators in vacuum: review of the phenomena and techniques to improve holdoff voltage, Trans. Electr. Insul. 28 (1993) 512–527, http://dx.doi.org/10.1109/14.231534.
[27] A.S. Pillai, R. Hackam, Optimal electrode-solid insulator geometry with accumulated surface charges, IEEE Trans. Electr. Insul. 19 (1984) 321–331, http://dx.doi.org/10.1109/TEI.1984.298806.
[28] S.A. Boggs, Partial discharge III: cavity-induced PD in solid dielectrics, IEEE Electr. Insul. Mag. 6 (1990) 11–20, http://dx.doi.org/10.1109/57.63094.
[29] N.C. Jaitly, T.S. Sudarshan, Novel insulator designs for superior DC hold-off in bridged vacuum gaps, IEEE Trans. Electr. Insul. 22 (1987) 801–810, http://dx.doi.org/10.1109/TEI.1987.298943.
[30] J.B. Andersen, V.V. Solodukhov, Field behavior near a dielectric wedge, IEEE Trans. Antennas Propag. 26 (1978) 598–602, http://dx.doi.org/10.1109/TAP.1978.1141899.
[31] Y.P. Chiou, C.H. Lai, C.H. Du, H.C. Chang, Finite-difference modeling of dielectric waveguides with corners and slanted facets, J. Lightwave Technol. 27 (2009) 2077–2086, http://dx.doi.org/10.1109/JLT.2008.2006862.